Cement and Concrete Research 40 (2010) 1429–1440

Contents lists available at ScienceDirect

Cement and Concrete Research

journal homepage: http://ees.elsevier.com/CEMCON/default.asp

Environmental effects on cover cracking due to corrosion

I. Balafas [a,*], C.J. Burgoyne [b]

[a] Department of Civil & Environmental Engineering, University of Cyprus, PO Box 20537, 1678 Nicosia, Cyprus
[b] Department of Engineering, University of Cambridge, Trumpington Street, Cambridge, CB2 1PZ, UK

ARTICLE INFO

Article history:
Received 14 July 2009
Accepted 12 May 2010

Keywords:
Cover cracking [B]
Corrosion [C]
Chlorides [D]
Environment [E]

ABSTRACT

This paper examines the environmental conditions under which the time to cracking of concrete, due to pressure caused by rust production on the surface of steel bars, is short. To determine this time, volume compatibility is assumed, which allows for compaction of all materials affected by the pressure, including the rust itself. A fracture mechanics concept is also used to signal cover failure. The model reveals that time-to-cover-cracking is a function of the rust production and the strength of the system to resist the resulting pressure. It is found that the highest corrosion rates are towards the end of autumn and the beginning of spring, when humidity reaches relatively high values with moderate temperatures. On the other hand the highest resistance of the system to corrosion production is during summer, since the humidity is low. In addition, rust pressure drops during summer due to creep; water moves out of the concrete which also deforms, giving more space into which the rust can expand. Structures exposed to humid summers would suffer from high rust production and rapid cover spalling. The model can assist in the decision-making process to identify when a bridge is more likely to corrode, which could indicate that new materials, like fibre reinforced polymers might be the most suitable design solution despite their higher initial cost.

1. Introduction

Steel works remarkably well with concrete; the strain capacities and strengths automatically lead to balanced sections with reasonable amounts of reinforcement. But there is a major problem with rust; extensive use of de-icing salts on bridges leads to corrosion of the reinforcement. 15 million tons of de-icing salts are used each year in the United States of America and 4 to 5 million tons in Canada [1].

When there is significant exposure to salt on the concrete surface, the alkaline protection to the steel can break down rapidly due to chloride attack and it may start to corrode; this can result in large and increasing portions of government budgets being spent to repair the concrete infrastructure.

New materials such as glass, carbon and aramid fibres have recently been introduced as alternative reinforcement to concrete; they are expensive but, if long-term costs are taken into account, the economic picture changes dramatically [2,3].

Nevertheless, it is not reasonable to expect all forms of construction to change because some concrete bridges have corrosion problems. Tools are needed to identify those structures which are likely to have problems and to apply sensible whole-life costing procedures to those structures; sensible decisions can then be made at the time that contractors bid to provide a structure.

The structural lifetime of a bridge exposed to deicing salts has two phases: time to corrosion initiation and time to cover cracking. Once the cover is cracked the corrosion is visible on the surface and this is often taken as the time when serious consideration is given, either to downgrading the bridge's load capacity, repairing it, or even replacing it.

Recently a model was developed to determine the time it takes to crack the cover after corrosion has begun under controlled environmental conditions [4]. This paper extends the model to include actual environmental exposures. Applications of the model can reveal the environmental conditions under which the time-to-cover-cracking is short. This can assist in the decision-making process that will identify when a bridge is more likely to corrode, in which case new materials may be the most suitable design solution.

The corrosion products of steel have a greater volume than the metal, and as a result a pressure is exerted on the cover, which eventually leads to spalling.

Cover spalling is obviously a function of the environment to which the bridge is exposed. Models to determine time-to-cover-cracking exist [5–8]. Those models try to predict times to cover failure of specimens under accelerated corrosion. But there are no models that introduce environmental parameters in the calculations. This paper identifies the particular circumstances when high corrosion rates will occur.

The model presented in the paper also improves existing forecasts. It introduces a volume compatibility condition that allows for the compaction of all materials that contribute to cover spalling, including the rust.

* Corresponding author.
E-mail addresses: ibalafas@ucy.ac.cy (I. Balafas), cjb@eng.cam.ac.uk (C.J. Burgoyne).

0008-8846/$ – see front matter © 2010 Elsevier Ltd. All rights reserved.
doi:10.1016/j.cemconres.2010.05.003

A new condition for signaling cover failure is also established, based on fracture mechanics and strain energies. Moreover, a new formula is proposed for the rate of rust production. That formula is based on Faraday's law and on work by Liu and Weyers [9]. Finally the mathematical formulation of rust composition is updated, based on recent experimental data on corrosion products in concrete.

The paper ends with a parametric study that shows which parameters have most effect on the time to failure, which can lead to future research.

2. Background

Cover cracking due to corrosion is a well known problem and a number of models to simulate the effects of rust in the concrete cover can be found in the literature.

Bazant [10] was the first to consider the problem. He used thick-wall-cylinder formulae to evaluate stresses generated by the rust, but he assumed that the cover fails with the first appearance of a crack on the inner surface of the cylinder.

Molina et al. [11] used finite elements to model cover cracking. It was a good early modelling attempt, but it made a number of simplifying assumptions. The rust production rate was assumed to be constant; the long-term properties of concrete were not taken into account and compaction of the rust was not properly introduced.

Liu and Weyers [9] performed experiments on concrete slabs and used thick-wall theory for elastic and partially cracked cover to model cover cracking. They proposed a formula for rust production that takes into account the reduction in rust production rate as the rust layer thickens. The phenomenon is well known [12,13], but their formula gives unrealistically high values of rust production at early ages when concrete resistivity is low. Liu and Weyers' model formulation does not take into account rust compaction or the crack space available for filling with rust.

Perez [14] extended the thick-wall formula, but did not study the cracked part of concrete in detail. He introduced compatibility conditions but did not properly model rust compaction and the model gives short times to cover cracking. Pantazopoulou and Papoulia [7] then introduced the Liu and Weyers formula for rust production and focussed on detailed modelling of cracked concrete. They introduced concrete softening and allowed for the crack presence, which gave space where the rust could be accommodated; the result was reduced pressure on the cover and longer times to failure. They analyzed the behaviour of the cover using Finite Differences. Other models appear at a later stage following similar lines [7] using thick-wall-cylinder formulae [15,16]. These formulae were updated by introducing stiffness changes due to rust presence, which altered the raised pressure in the system [17].

Finally, fracture mechanics have been implemented to model cover cracking [18,19]. The intention of those models was not to give good time predictions but to enhance understanding of crack initiation and propagation inside the cover.

From the preceding it is obvious that a number of efforts exist in the literature to forecast time-to-cover-cracking. The models use thick wall cylinder analysis or fracture mechanics. As cover fails due to crack propagation an analysis is needed to combine both stress and fracture mechanics analysis; stress evolution can be given from a thick wall cylinder analysis and a fracture mechanics concept can be developed to signal unstable crack propagation and cover failure. In addition proposed rust production formulas are either linear (based on Faraday law) or non-linear which give non-pragmatic high production rates at low age. According to test results rust production is linear at early ages whereas grows non-linear at latter stages [12,13,20]. Rust mechanical properties are not yet well understood as they are difficult to measure but recent tests [21,22] shed some light in to this aspect and can be used in proposed models.

3. Research contribution

The models described in Section 2 try to mimic laboratory tests performed under controlled conditions. As the main motivation of this work is to determine the environmental conditions under which time-to-cover-cracking is short, a model has been developed to forecast such times under given environmental conditions.

The newly developed model is based on the models outlined in Section 2 and focuses on details that need to be improved. It proposes a new volume compatibility condition to determine the pressure that arises due to the presence of the rust. This condition allows for the proper compaction of all materials affected by the pressure on cover, including the rust itself. As the cover fails due to crack propagation, a fracture mechanics approach is used, based on strain energies, to signal cover failure. A new rust production formula is proposed, based on the linear Faraday law and the non-linear Liu and Weyers proposal [23]. It also proposes a modification to a formula proposed by Lopez et al. [24], which relates concrete resistivity to humidity. This modification introduces an increase of concrete resistivity near saturation. This is combined with a corrosion rate formula proposed by Liu and Weyers [9]. Attention is also paid to the mechanical properties of the rust. Data from papers which look at the microstructure of rust are used to evaluate the rust properties that are crucial for this analysis i.e. volume expansion, density and bulk modulus [21,22]. As the motivation of this work is to identify the environmental conditions under which time-to-cover-cracking is short, the environmental effects on rust production and concrete (short and long term) properties were carefully introduced.

4. Time to cracking model

After corrosion initiation, hydrated rust accumulates around the bar, causing pressure and leading to cover cracking. The ability to predict the time to cover-cracking is important because it marks the end of structure's fully-effective service life.

To predict the damage caused by corroding reinforcing bars, knowledge of the state of stress in the surrounding concrete is required; this can be determined by means of a concrete ring model, which will be described later. The radial stresses on the concrete result from the volume increase of hydrated red rust, can be regarded as a uniform pressure acting on the inside of a thick-walled concrete ring, whose thickness is determined from the thinnest concrete cover around the bar, which gives the shortest crack path from the bar to the free surface. The concrete ring approximates the effect of surrounding concrete, but due to different geometry between the cover ring model and the real cover, the stresses will only approximately correspond to the stresses in the real situation. However, the critical tensile stresses at the thinnest section are likely to be reasonable so the concrete ring model can be accepted for the analysis [5,25,26].

5. Active corrosion

Once the chloride concentration at the reinforcing steel reaches a specified threshold, a difference in electrical potential on the steel surface is established, and a corrosion cell is formed (Fig. 1). The corrosion current which flows in the cell is governed by the resistances that result from:

- the iron dissolution rate in the anode (R_A),
- the oxygen and water availability in the cathode (R_C), which are converted into hydroxyl ions,
- the transport rate of the hydroxyl ions through concrete which acts as an electrolyte ($R_{c,res}$).

The resistance of the steel (R_{st}) is negligibly small compared to the other active resistances.

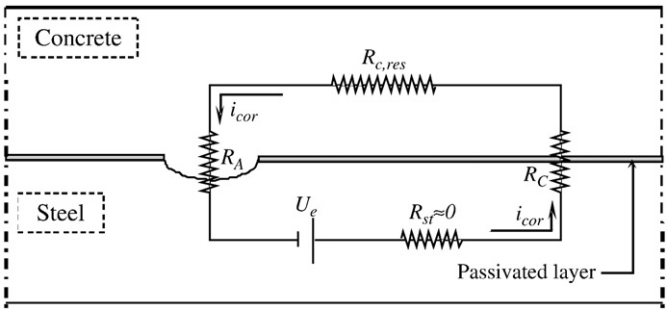

Fig. 1. Simplified electrical circuit model for the corrosion of steel in concrete [27].

Corrosion stops if one of the three resistances is infinite. This happens under three circumstances:

- when the steel is passivated ($R_A \to \infty$)
- oxygen is not available at the cathode, e.g. underwater structures ($R_C \to \infty$), or
- concrete is totally dried out ($R_{c,res}$, $R_C \to \infty$).

The value of R_A is a function of time due to increasing thickness of rust. The ionic diffusion distance increases and rate of rust formation decreases [7,28], but there is only limited data available from experiments.

Under partially saturated conditions, which are predominant in highway bridges, corrosion rates are extensively dependent on the concrete electrolytic properties ($R_{c,res}$) that govern the transport of negatively charged ions from cathodic to anodic areas. The transfer of those ions are mainly through the pore water, so the pore structure characteristics of the concrete, the degree of water saturation and the total ionic concentration of the pore solution are relevant factors affecting the ion movement and therefore the corrosion propagation [24,29–31].

Experiments have shown that corrosion rates are very slow at low relative humidity (<50%) and essentially corrosion stops below 35%. The rate increases exponentially from 50% to 70%; it remains nearly constant from 70% to 90% and decreases from 90% to complete saturation, due to oxygen limitation at the cathode [24,29,30,32,33].

Corrosion is also affected by temperature. At high temperatures, water content decreases, but on the other hand ions become more mobile and salts become more soluble. At the low end of the temperature scale the pore water will freeze and corrosion stops as the ions can no longer move [34].

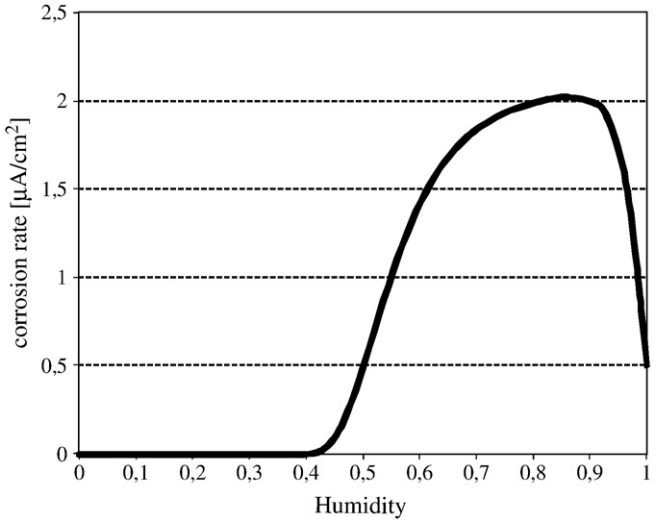

Fig. 2. Relationship between corrosion rate and relative humidity for a concrete element with Cl^- content 1.8 kg/m^3 under temperature 23 °C and age 1 year.

The above effects are included in a formula introduced by Liu and Weyers [9]. The formula is based on 2927 corrosion rate measurements from seven series of chloride contaminated specimens, covering exposure up to five-years. The chlorides had been introduced in the original mix. The corrosion rates, measured as corrosion current density, were correlated with temperature, concrete ohmic resistance, chloride content and exposure time by using a multiple non-linear regression model, as follows [9]:

$$i_{cor} = 0.0092 \exp\left(8.37 + 0.618 \ln\left(1.69 C_{fc}\right) - \frac{3034}{T} - 0.000105 R_{c,res} + 2.35 t^{-0.215}\right) \left[\mathrm{A/m^2}\right] \quad (1)$$

where C_{fc} is the free chloride content (kg/m^3), T is temperature at the depth of steel surface (K), $R_{c,res}$ is the ohmic resistance of the cover concrete (ohms), and t is time from initiation of corrosion (year).

Eq. (1) does not include the corrosion rate reduction at high humidity levels due to limited oxygen availability. Lopez et al. [24] have studied the above relationship. By fitting to their published experimental data, $R_{c,res}$ can be given as a function of relative humidity (h):

$$R_{c,res} = 90.537 \cdot h^{-7.2548} [1 + \exp(5 - 50(1 - h))] [\mathrm{ohms}] \quad (2)$$

$R_{c,res}$ from Eq. (2) can then be substituted into Eq. (1) to give the corrosion rate; Fig. 2 shows the relationship between corrosion rate and relative humidity for a one year old concrete element with Cl^- content 1.8 kg/m^3 at 23 °C.

Corrosion rate is strongly affected by the environmental conditions and time of exposure. Liu's formula (1) is the only formula found in the literature, although results from such laboratory tests normally give higher rates than those taken from real structures [7,35]. More long term corrosion tests are needed to establish relationships between corrosion rates and environmental properties.

5.1. Rust properties

Several papers have studied the properties of rust formed on bars embedded in concrete [22,36–41]. The properties that are of interest for this work are the chemical composition, together with the percentage by weight, the density and the volume of each chemical component. Although in all the cited work the chemical composition of rust and the mass properties are determined, only Suda et al. [22] have reported values for percentage and volume of each chemical component in the final product. Note that the volumetric ratio of rust in relation to that of steel is the most important parameter as it is the one responsible for cover cracking. Hence, Suda's results are used in this work and are shown in Table 1.

According to Suda, rust formed on bars embedded in concrete consists of magnetite (Fe_3O_4), geothite (αFeO(OH)), lepidocrocite (γFeO(OH)) and amorphous components ($Fe(OH)_3$ and FeOOH). Knowing the percentage, density and volumetric ratio of each chemical component in relation to steel, the density and volumetric ratios of rust in relation to that of steel (r_d and r_V) can be found. On the table the mass ratio of iron to that of rust r_m, is also shown.

Due to scatter of values for geothite's density and volumetric ratio, lower and upper values are determined for rust properties. Average values, shown in bold in the table, are used below. The results show that the average volumetric ratio r_V is close to 3, which is lower than the values given in [6–8], where for cover cracking calculations the ratio is taken between 3.6 and 4. However, the value of 3 agrees with recent published data on rust composition evaluation [36,41]. A parametric study below will reveal the affect of r_V.

Since rust will be under compression between steel and concrete, the mechanical properties of rust, such as its elastic and bulk moduli, are needed. Because those properties were unknown, rust has traditionally

been assumed to behave like liquid water with bulk modulus 2.00 GPa [7,11,14]. Recently, Konopka has tested specimens of rust and measured a range of 40–87 MPa for the elastic modulus and 0.48–0.54 GPa for the bulk modulus [21]. In the absence of other tests on the elastic properties of rust, Konopka's values are used in this work.

5.2. Corrosion build-up

Faraday's law, which states that the rate of electron flow to or from a reacting interface is a measure of reaction rate, is often used to relate the mass of steel eroded M_s over time, which is transformed to rust, to the current density i_{cor} (A/m^2) that flows through the electrochemical corrosion cell:

$$\frac{dM_s}{dt} = \frac{i_{cor}A}{n_r F}\left[\text{mole}/\left(\text{m}^2\text{s}\right)\right] \tag{3}$$

where F is the Faraday constant (=96494 A s/mol e$^-$) and A is the atomic weight of the iron being dissolved (for Fe, A=0.05585 kg/(mol Fe)) and n_r is the valency of the reaction which is given in mol e$^-$/mol Fe. The valency in any given reaction should be an integer and is usually taken empirically as 2.0 mol e$^-$/mol Fe. That value assumes incorrectly that all corrosion products are $Fe(OH)_2$. The Fe valency from Suda's results (Table 1) would give n_r about 3, due to the presence of many different rust compounds. However, Faraday's Law gives good agreement with test results when n_r=2, so that value is used here [5–7,14,42]. By substituting those values the annual corrosion rate is given from:

$$\frac{dM_s}{dt} = 9.127 i_{cor}\left[\text{kg}/\left(\text{m}^2\,\text{year}\right)\right] \tag{4}$$

The rate of rust production (dM_r/dt) can be given from the rate of steel consumption (dM_s/dt):

$$\frac{dM_r}{dt} = \frac{1}{r_m}\frac{dM_s}{dt} = \frac{9.127 i_{cor}}{r_m}\left[\text{kg}/\left(\text{m}^2\,\text{year}\right)\right] \tag{5}$$

where r_m is the mass ratio of iron to that of rust, and M_r is the mass of rust. If the diameter of a corroding bar is ϕ then the total mass of consumed steel per unit length of bar for a given period of active corrosion time t_{cor} is given from:

$$M_s = 9.127\pi\phi\int_0^{t_{cor}} i_{cor}dt\,[\text{kg}/\text{m}] \tag{6}$$

As the rust layer thickens, the iron ionic diffusion distance increases, so the diffusion rate goes down and the rate of rust production decreases. Liu [23] performed experiments on slab specimens and proposed the formula below to allow for rust mass rate reduction with time:

$$\frac{dM_r}{dt} = \frac{k_p}{M_r} \Rightarrow M_r = \left[2\int k_p dt\right]^{1/2}[\text{kg}/\text{m}] \tag{7}$$

where k_p is an empirical coefficient related to the rate of metal loss and is given from:

$$k_p = k_{coef}(1/r_m)\pi\phi i_{corr} \tag{8}$$

ϕ is expressed in m and i_{corr} in A/m^2, while k_{coef} is a coefficient that allows for the reduction of corrosion rate with rust thickness; it has not been studied so is typically evaluated by fitting the proposed models [7,8,23,43] to published experimental data by Liu on concrete slabs with bars under uniform corrosion [6]. Work to study the rate of rust production in relation to rust layer thickness is needed.

Eq. (7) assumes that the rust layer formed is uniformly distributed and the diffusion properties are the same across the thickness of the rust layer. Examination of corroded bars embedded in concrete, under natural exposure, showed that the corrosion products form two layers [20,37,38,44]. Although the composition of the two layers is found to depend on the environmental exposure [45], in all cases the inner layer was found to be denser than the outer. For layers of rust, with varying diffusion properties through thickness, Eq. (7) is transformed [6,20,46] to:

$$\frac{dM_r}{dt} = \frac{k_p}{M_r^{n_l}} \Rightarrow M_r = \left[n_l\int k_p dt\right]^{1/n_l}[\text{kg}/\text{m}] \tag{9}$$

in which the coefficient n_l takes values between 2 and 3 (2 for rust with uniform density across the thickness). As n_l increases from 2 to 3 the non-linearity of the rust production versus time increases. Values for k_p are dependent on n_l; they decrease while n_l increases from 2 to 3.

Both the Faraday law (4) and Liu and Weyers' formula (9) have disadvantages. Eq. (4) does not include the presence of a gradually thickening protective rust layer. On the other hand, Eq. (9) gives unrealistic corrosion rates at short times.

Tests on corrosion propagation mechanisms have also revealed two phases: the kinetic and the non-linear diffusion [12,13,20]. During the kinetic phase the rust production versus time is linear. When the thickness of the layer of corrosion products grows enough, the rate of rust production decreases and is dependent on the rust layer diffusion properties.

To include the above observations in the present work, a combined rule is adopted, where it is assumed that initially the corrosion rate is constant, following Faraday's law (4), but when the corrosion rate of

Table 1
Properties of rust formed on bars embedded in concrete [22].

Component	Percentage by weight [%]	Density [gr/cm^3] Lower bound	Density [gr/cm^3] Upper bound	Volume expansion ratio vol. component/vol. Fe Lower bound	Volume expansion ratio vol. component/vol. Fe Upper bound
Magnetite [Fe_3O_4]	12	5.2		2.1	
Geothite [αFeO(OH)]	15	3.3	4.3	2.9	3.8
Lepidocrocite [γFeO(OH)]	12	4.1		3	
Amorphous components [$Fe(OH)_3$ and FeOOH]	69.6	4		3	

	Lower bound	Upper bound	Average
r_V	2.90	3.03	2.96
Rust density [g/cm^3]	4.04	4,19	4.12
Steel density [g/cm^3]	7.85		
r_d	1.942	1,872	1.907
r_m	0.670	0,618	0.643

Eq. (9) is lower than Eq. (4), the corrosion rate is evaluated using Eq. (9) (Fig. 3). Hence, the consumed mass versus time can be given by:

$$M_s = \min\left(M_{s,FL}, r_m M_{r,LW} - M_{diff}\right)[\mathrm{kg/m}] \quad (10)$$

in which $M_{s,FL}$ is the steel mass consumed according to the Faraday law (6), $M_{r,LW}$ is the rust produced according to Liu and Weyers formula (9) and M_{diff} is given from:

$$M_{diff} = \begin{cases} r_m M_{r,LW} - M_{s,FL} & \text{for } r_m \dfrac{dM_{r,LW}}{dt} < \dfrac{dM_{s,FL}}{dt} \\ 0 & \text{for } r_m \dfrac{dM_{r,LW}}{dt} > \dfrac{dM_{s,FL}}{dt} \end{cases} \quad (11)$$

where $dM_{r,LW}/dt$ is the rate of rust productions according to Eq. (9), and $dM_{s,FL}/dt$ is the rate of consumed steel according to Eq. (6). Both $dM_{r,LW}/dt$, $dM_{s,FL}/dt$ can be determined numerically.

By fitting Eq. (9) to published data by Liu [6] values of k_p for various n_l are shown in Table 2.

6. Pressure on cover

The following analysis assumes that the steel bar is surrounded by a cylinder of concrete, whose thickness equals the minimum distance from the bar to the air (Fig. 4(a)). The concrete quality in the cylinder is assumed to be uniform. Corrosion is assumed to take place at a uniform rate all round the bar.

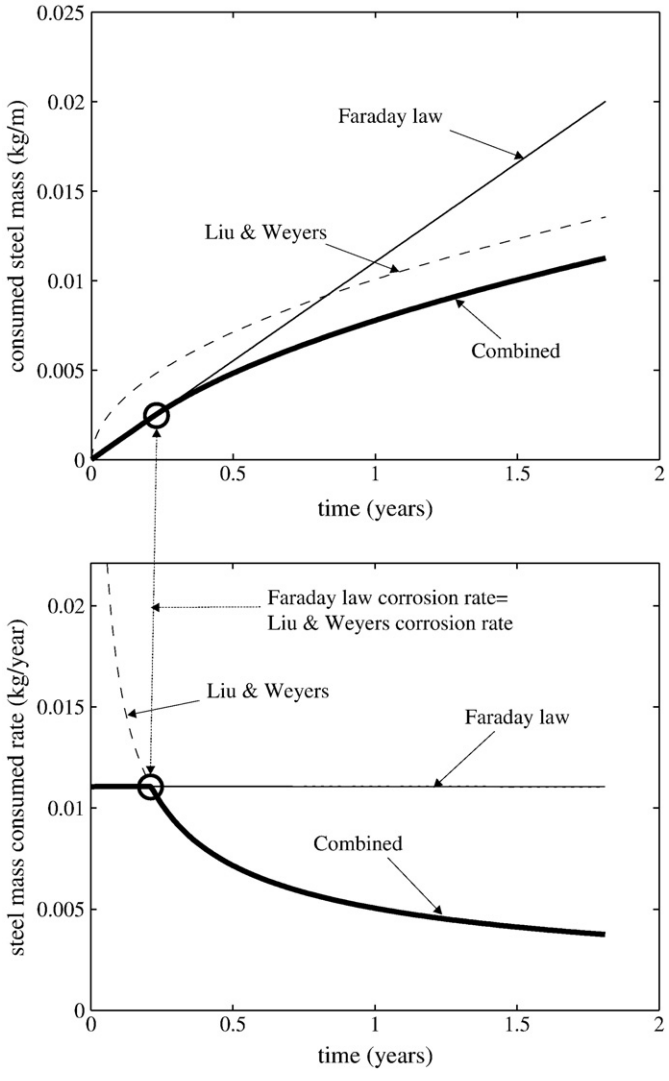

Fig. 3. Steel consumed and rate of consumed mass versus time following Faraday law (4), Liu and Weyers formula (7) and combination of the two ($n_l = 2$).

Table 2
Values of k_p on given n_l.

n_l	k_p
2.00	0.086
2.25	0.036
2.50	0.0154
3.00	0.00324

The rust is larger than the steel (Fig. 4(b)). It expands into the pore spaces and then exerts pressure on the surrounding concrete, which behaves like a thick cylinder under internal pressure (Fig. 4(c)). Clearly, knowledge of the rate at which the rust expands, and the volume of pores to be filled, are crucial to the determination of the time at which the radial pressure starts to develop. The stresses on the inside of that cylinder eventually reach the tensile strength of the concrete, which then cracks. The cylinder then consists of two zones, an inner cracked zone where the tangential stresses are zero, and an outer solid cylinder (Fig. 4(d)).

The analysis takes account of the compressive strains on the steel bar, the rust, the cracked ring of concrete and the uncracked ring of concrete, all caused by the radial pressure generated by the rust. Since the process is slow, account is also taken of the creep strains that are induced. Compatibility conditions, between the amount of rust produced by the corrosion and the volumetric changes that arise from the material strains, allow the evolution of the process to be followed. Details can be found in [4].

It has to be noted here that Fig. 4(d) shows a symmetrical propagation of cracks in the cover, which would be expected from uniform corrosion. In reality corrosion on the bars may not be uniform, and non-symmetrical crack propagation may be observed. Realistic non-symmetrical rust production and pressure generation around the bar, which will cause a non-symmetrical crack propagation, may change the time-to-cover-cracking. In such cases times-to-cover-cracking are expected to be shorter hence uniform rust generation around the bar predictions is conservative.

Tests have also been performed in which local pitting corrosion is induced on bars embedded in concrete [47,48]. The tests aimed to control the bars corroding length and had only a fraction of the steel length to corrode. This was achieved by embedding in concrete mechanically continuous bars, which had a center segment made of carbon steel and two PVC or stainless steel segments for the remainder. The center carbon steel segments were relatively short in the order of 20–60 mm. The observed times to cover cracking were shorter in comparison to model's predictions. Although the applicability of those tests in real situations may be questioned as corroding lengths of 20–60 mm are considered too low, nevertheless it has been concluded in [4] that model applications are limited to cases in which relatively long corrosion lengths are expected along the bars.

The final breakthrough of the critical crack occurs when the strain energy released as the crack propagates to the surface exceeds the fracture energy of the new crack surfaces formed. This marks the moment when the cracking becomes visible to inspectors and this is the time when concerns will (or at least should) be raised about the strength and longevity of the structure.

6.1. Partially cracked ring model

When a crack initiates at the interface between bar and concrete it will fully propagate through the cover only when the tensile concrete capacity of the ring is exhausted. Thus the concrete will be cracked at places where the tangential stresses have exceeded f_t and uncracked in the outer part of the cylinder where the stress is less than f_t.

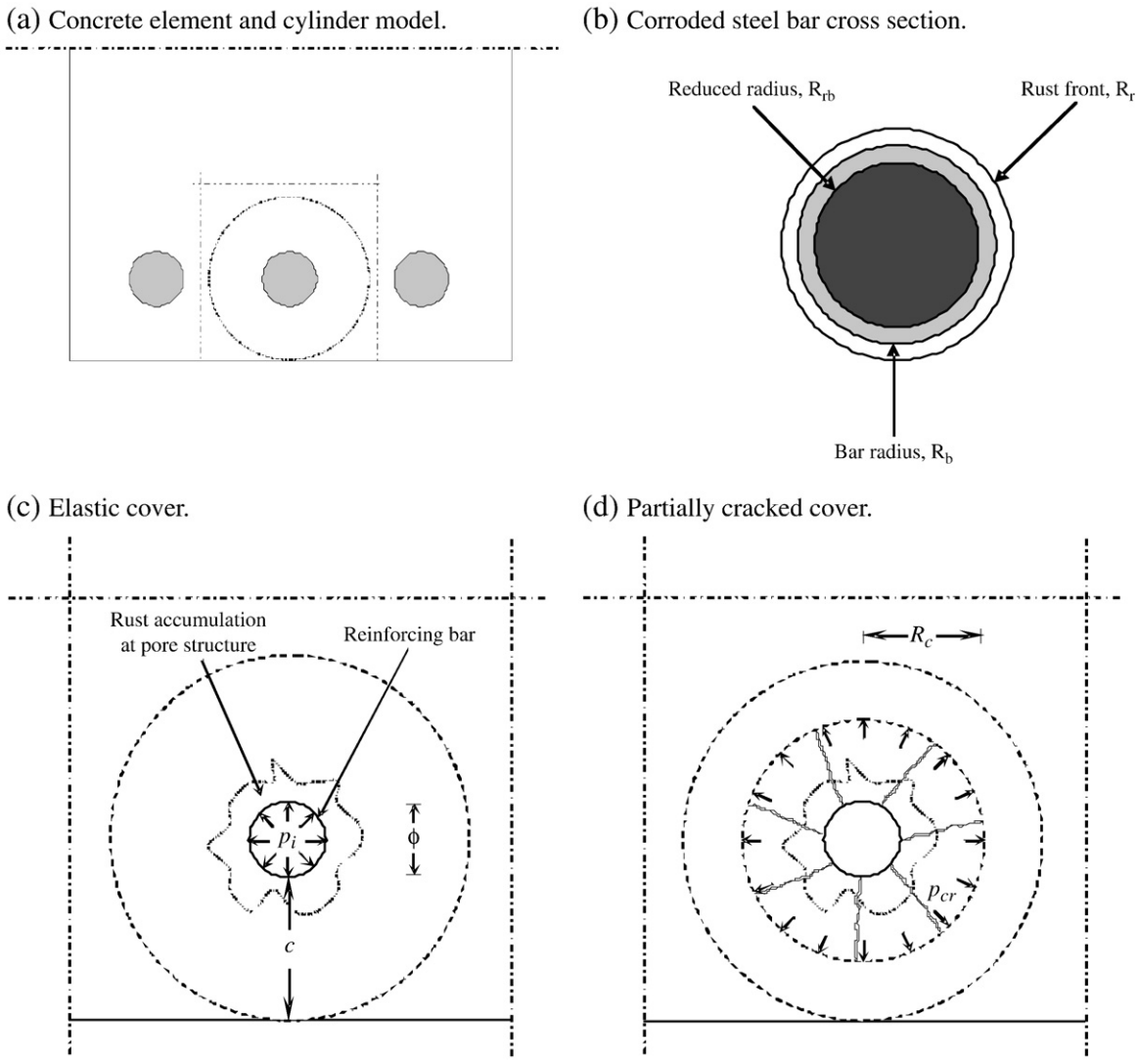

Fig. 4. Idealisation of cover concrete as a thick walled cylinder.

The newly cracked concrete takes the form of teeth, and the cracks between them form more voids into which the rust can expand. The radial pressure in the concrete teeth, and the corresponding strain, are governed by the pressure in the rust, while the tangential strain in the teeth is assumed to vary linearly from zero on the inner surface of the teeth to that on the inner surface of the uncracked outer ring. The outer ring still behaves as a thick-walled elastic cylinder. Balafas et al [4] showed that by setting up suitable equilibrium and compatibility conditions, and using the assumed elastic properties of the concrete and the rust, it is possible to find the radius of the crack front R_c as the root of:

$$f_t R_c^3 + (R_{rb} + t_{rc}) p_i R_c^2 - [c + (R_{rb} + t_{rc})]^2 f_t R_c + [c + (R_{rb} + t_{rc})]^2 (R_{rb} + t_{rc}) p_i = 0 \quad (12)$$

from which the root $R_{rb} + t_{rc} \le R_c \le (R_{rb} + t_{rc}) + c$ is chosen for the crack front. c is the cover thickness, R_{rb} is the reduced bar radius due to corrosion and t_{rc} is rust's thickness while compressed with pressure p_i.

7. Cover failure

As pressure increases, cracks propagate through the cover; experiments have shown that although, at the early stages of crack propagation several cracks appear, by the end of the test there is a single crack that finally breaks the cover [18,49] on the weakest side of the concrete element. When this crack appears there is an effect of stress relaxation that stops the propagation of the other internal cracks [49].

To determine when this single crack propagates unstably through the cover, fracture mechanics concepts can be employed. As existing cracks extend, the energy needed to form associated new surfaces, depends on the interface fracture energy, and must be compared with the energy released by the system, which in turn depends on the change of the strain energy stored in the system [50,51].

A crack will finally extend to fail the cover only when the energy release rate G_R is greater than the fracture energy of concrete G_F ; if not there is insufficient energy for the flaw to propagate [50].

8. Model application

A numerical model was built which could be applied to real conditions with annual humidity and temperature fluctuations and corrosion may appear over relatively long lengths (>60 mm) along the bars. Consider a concrete cover with properties shown in Table 3, which also shows the environmental conditions that for the purpose of this analysis are assumed to vary sinusoidally through the year. It is accepted that this is a gross simplification of the real situation, but it allows some basic inferences to be drawn. Corrosion production is

Table 3
Model inputs for cover cracking evaluation.

Concrete properties	
Thickness, c [mm]	50
Compressive strength, f_c [N/mm^2]	30
Tensile strength, f_t [N/mm^2]	3.28
Elastic modulus, E_c [KN/mm^2]	31.9
G_F [N/mm]	0.12
Rust properties	
E_r [N/mm^2]	60
K_r [kN/mm^2]	0.5
r_m	0.643
r_V	2.964
r_d	1.907
n_l	2.00
k_{coef}	0.086
t_{fill} [μm]	8
Steel properties	
Bar diameter, ϕ [mm]	16
Density, p_s [kg/m^3]	7850
Elastic modulus, E_s [KN/mm^2]	210
Environmental properties	
Annual relative humidity range [%]	40–85
Annual temperature range [°C]	(−5)–(+35)
Time to corrosion initiation [years]	30

assumed to follow the combined Faraday Law–Liu and Weyers relationship (Section 5.2).

In Fig. 5 the change in corrosion rate with time is shown. The lowest corrosion rate at mid summer is due to low relative humidity but the highest corrosion is not at mid-winter, as might be expected, since the temperature is then low. The two annual i_{cor} peaks take place at the end of autumn (fall) and the beginning of spring.

Fig. 6 shows the pressure build-up on the cover due to the rust. Three curves are shown; the top is the pressure at the rust–concrete interface while the lower two curves describe pressure development at the crack front with and without taking into account tension softening of concrete. It is clear that tension softening has little practical effect. In the early stages after corrosion initiates, the pressure is zero as the rust is consumed filling the pores around the bar. The pressure then builds but fluctuates; it drops during the summer when the concrete dries while creep deformations increase the available space for rust. In the winter the rust production rate increases.

Fig. 7 shows the variation of concrete resistivity with time; as expected, it is highest during summer because of the low humidity.

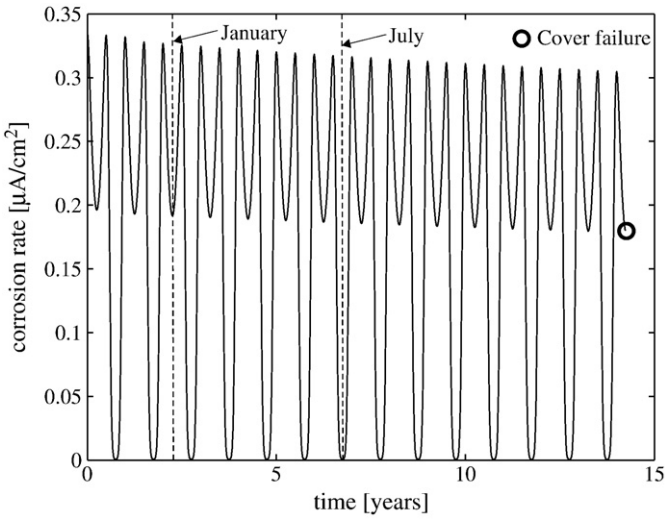

Fig. 5. Corrosion rate versus time.

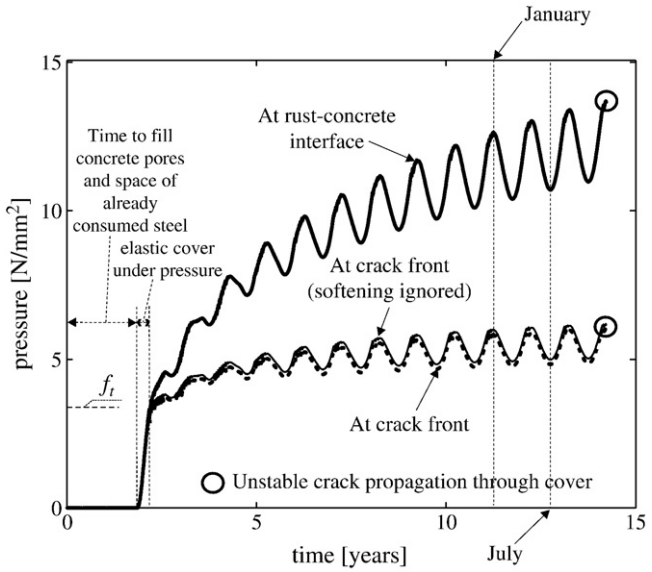

Fig. 6. Pressure built-up versus time at crack front and at rust–concrete interface with and without taking into account softening of concrete in tension.

In Fig. 8 the mass of steel consumed is shown, according to Faraday's Law and the combined rule (10). The point where the slope of the Faraday law equals that of the Liu and Weyers formula (7) is presented. From that point onwards the combined rule departs from the Faraday Law to Liu and Weyers formula. The rust mass production according to the combined rule is also drawn. In addition, Fig. 9 shows the steel mass consumption rate versus time. At early ages the Liu and Weyers formula predicts substantially higher consumption rates, which reduce to values lower than those given by the Faraday law after 4 years of corrosion. It can also be observed that the consumption rates are minimum during summer while they reach their maximum values towards the end of autumn and the beginning of spring.

The change in the radii of the inner and outer surfaces of the concrete ring are shown in Fig. 10, which also shows the reduction in the steel bar radius, which is small due to the high modulus of the steel. The change of the inner concrete radius is much bigger than the outer.

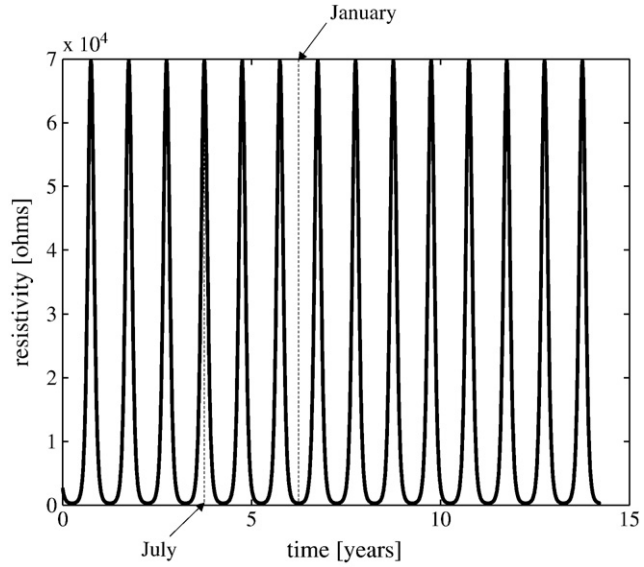

Fig. 7. Concrete resistivity versus time.

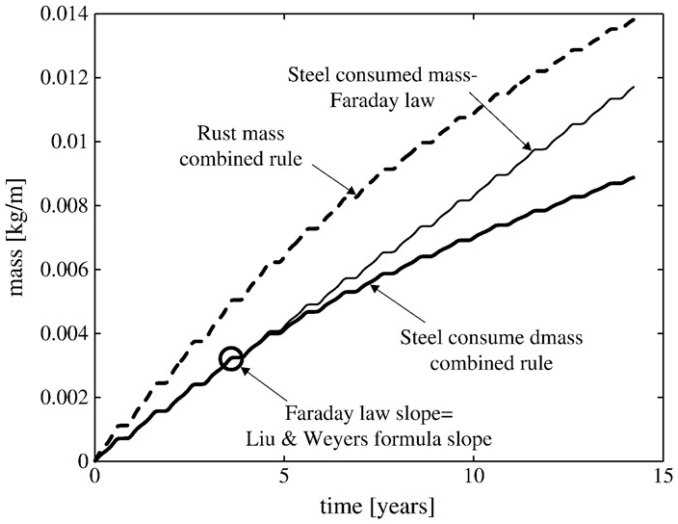

Fig. 8. Consumed steel and rust mass production versus time.

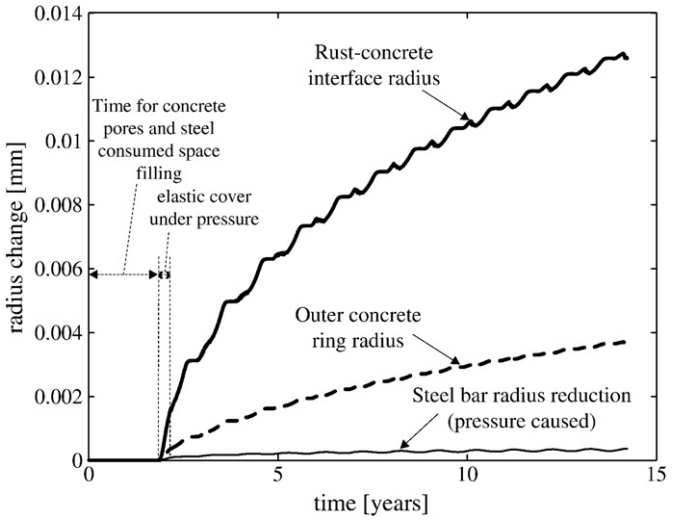

Fig. 10. Radius change of inner (rust–concrete interface) and outer concrete ring surfaces as well as steel bar radius reduction due to rust pressure only.

The propagation of cracks through the cover versus time is shown in Fig. 11, measured from the centre of the bar which has a radius of 8 mm. Several plateaus can be observed; these are due to an increase of creep deformation of concrete during the summer. The concrete expands due to water movement to the environment, which creates more space for rust to expand into, and corresponds to the drop in pressure shown in Fig. 6. The plateaus get longer as the concrete ages due to a slowing in the rate of rust production caused by thickening of the rust layer.

The strain energy built up in the cover ring versus time is important since it governs when final fracture takes place; it is shown in Fig. 12. Initially the strain energy is zero as pressure is zero, but again due to creep effects the strain energy drops during summer and the drops become more pronounced due to reduced rust production. When the strain energy reaches the critical value of the concrete's fracture energy, the cover can no longer support the pressure from rust and fails.

The total strain energy of the cover consists of strain energies from elastic concrete, cracked concrete and steel bar. Each contribution is shown in Fig. 13; the highest is from elastic concrete while the lowest is from cracked concrete in tension (under softening). The steel bar holds relatively high strain energy, despite the low deformations, due to its high Young's modulus.

Fig. 14 shows the build up of rust thickness with and without concrete pore filling. On the same graph the reduction of bar radius is also sketched. The difference between curves “rust thickness with pore filling” and “bar radius reduction” causes pressure on cover. The radial deformation of the cracked part of the cover, which occur due to the internal pressure causing radial strains is also drawn for comparison.

Finally, the total volume created to accommodate the rust within the concrete cover and its components can be found in Fig. 15. It can be observed that the space made available by steel for rust accommodation (mainly due to steel consumption, rather than steel contraction due to pressure) and the inner concrete perimeter radial expansion are the two basic components of the total volume. The volume formed in cracks and due to radial compression of the cracked part of the cover represent only a small portion of the available total volume. Although Fig. 10 showed that the radius change for the inner concrete radius was more than double that of the outer, Fig. 15 shows that the volumes created by the expansions of those perimeters are similar.

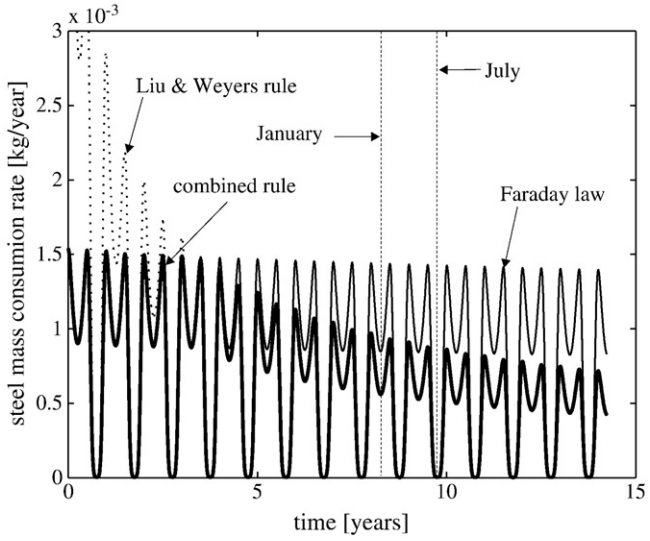

Fig. 9. Steel mass consumption rate versus time.

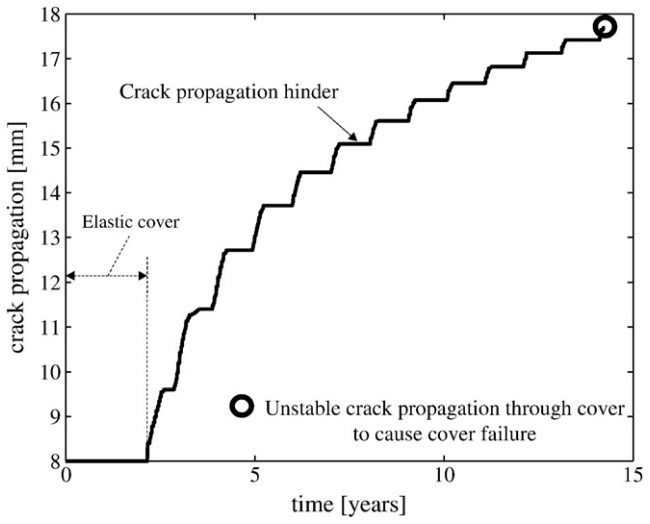

Fig. 11. Propagation of cracks in cover versus time.

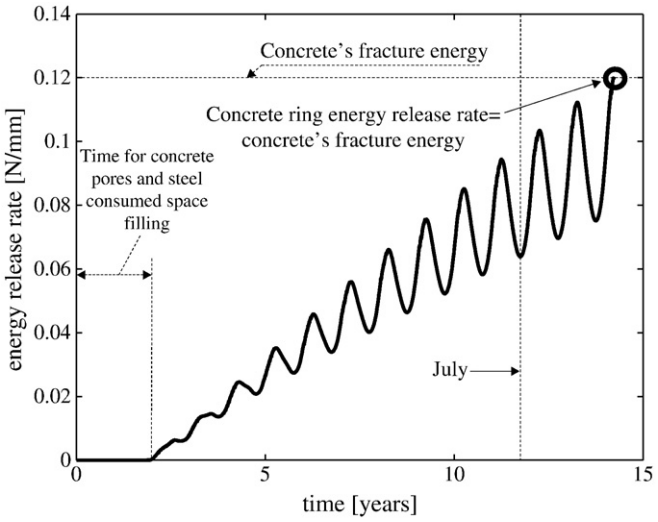

Fig. 12. Concrete ring energy release rate built-up (per metre length) versus time.

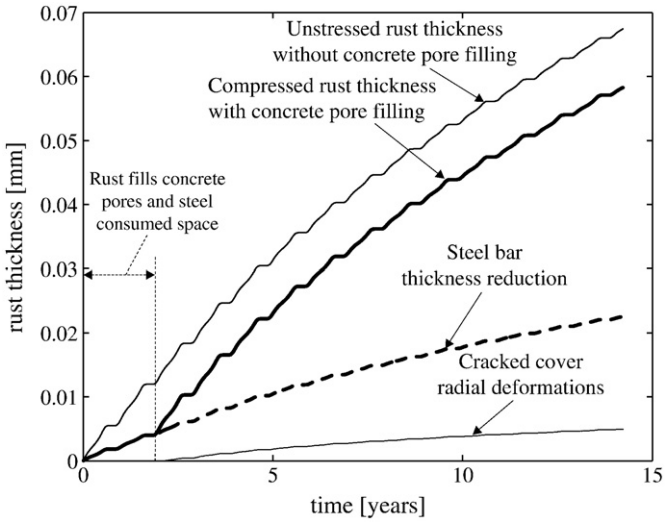

Fig. 14. Change of thickness for rust with and without concrete pore filling, steel bars and cracked compressed concrete, versus time.

9. Parametric study

The environment plays a role in controlling the time when the cover will crack. To study its influence, three different environmental conditions are defined for detailed study: these will be labelled mild, medium and severe. The properties of those conditions are described through chloride concentration, relative humidity and temperature as shown in Table 4. Temperature T and humidity h are assumed to vary sinusoidally according to:

$$h_{en} = \frac{h_{min} + h_{max}}{2} - \frac{h_{min} - h_{max}}{2} \sin(2\pi t) \quad (13)$$

$$T_{en} = \frac{T_{min} + T_{max}}{2} + \frac{T_{min} - T_{max}}{2} \sin(2\pi t) \quad (14)$$

where T_{max}, h_{max} and T_{min}, h_{min} are maximum and minimum annual temperatures and humidities respectively; t is in years. Note that the different sign in front of the second term in the two equations means that the highest temperature occurs with the lowest humidity, and vice-versa.

The de-icing salt's Cl^- concentration increases depending on the lowest temperature values. A 20% de-icing salt solution can depress the water freezing temperature to −16 °C. It is assumed that for "severe" environmental conditions a 20% Cl^- concentration solution is applied to the bridge (Table 4) since the temperature drops to −10 °C. 10% and 6.5% Cl^- concentration solutions are applied when the bridge is subject to "medium" and "mild" environments respectively, according to the low temperature values.

The times to cover cracking are 4.2, 6.2 and 7.2 years for mild, medium and severe environments respectively, which is counter-intuitive. The severe case gave the highest time to cracking because the average temperature is the lowest while the humidity reaches high values, when O_2 availability is limited. As a result, and with reference to Eq. (1), the average corrosion rates for mild, medium and severe cases are 1.918, 1.160 and 0.853 A/m^2 respectively. The higher corrosion rates can also be observed on Figs. 16 and 17. The build-up of strain energy and the rust production, are both faster under mild environmental conditions. Note on Fig. 17 that the critical mass of rust to crack the cover decreases from mild to severe environments. This happens because the average humidity with time drops from mild towards severe environment. Creep strains are then highest for mild conditions and the space available for rust to expand is more. Consequently, more rust is needed to create the appropriate pressure to crack the cover.

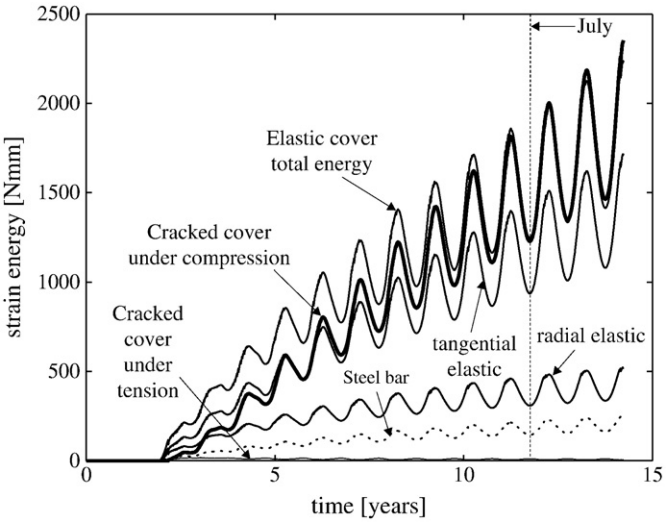

Fig. 13. Elastic concrete (radial and tangential), cracked concrete and steel bar strain energies (per metre length) versus time.

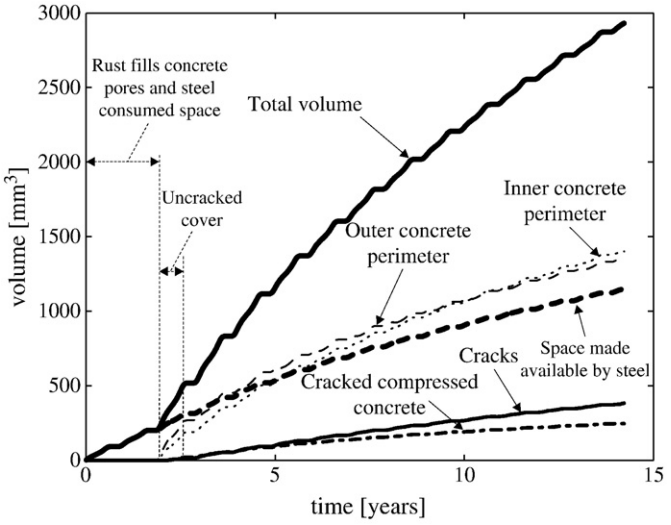

Fig. 15. Total volume created for rust accommodation in concrete cover and its components per metre length, versus time.

Table 4
Environment definition (T and h fluctuate according to Eqs. (13) and (14)).

Environment	Pore Cl^- concentration	Relative humidity		Temperature	
	[kg/m^3]	%		°C	
	(% by weight of salt in solution)	h_{min}	h_{max}	T_{min}	T_{max}
Mild	70 (~6.5)	50	85	0	50
Medium	100 (~10)	55	90	−10	30
Severe	230 (~20)	60	100	−15	20

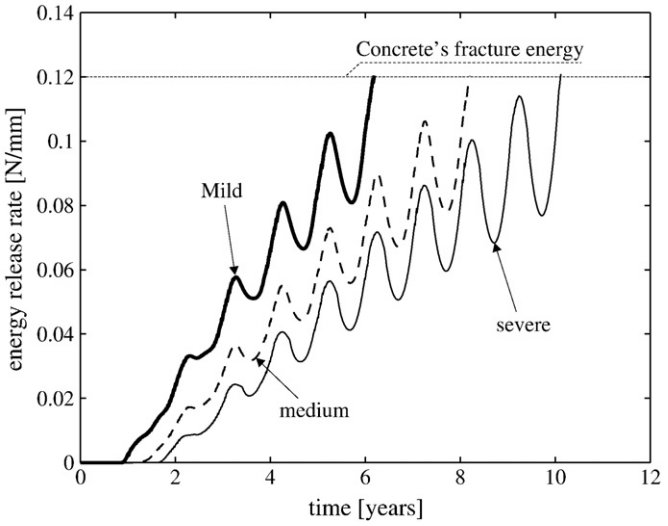

Fig. 16. Energy release rate build-up in cover under various environmental conditions, versus time.

The model also revealed that time to cover cracking decreased with increasing annual temperature. The same trend was observed with humidity up to ~90%, above which the time-to-cover-cracking increased due to limited O_2 availability (Fig. 2).

Concrete strength also influences the time when cover-cracking occurs. Three types of concrete were introduced to the model with the properties shown in Table 5. Time to cracking decreased when the concrete strength was increased. Stronger concrete is less porous, so less rust is needed to fill the pores around the steel bar, but more importantly it is stiffer. Thus the same rust mass exerts more pressure when put in a stronger concrete. This is illustrated in Fig. 18 where,

Table 5
Concrete properties and times to cover cracking.

Concrete cube strength [N/mm^2]	Equivalent rust thickness to fill pores [16] [μm]	Time to cover cracking [year]
30	8	14.2
40	6	10.2
50	4	8.1
60	2	6.1

when a similar rust mass was produced, a much higher strain energy was generated in stronger concrete.

The properties of rust have by far the highest effect on time-to-cover-cracking. Analyses were performed by changing one of the rust properties, while all the other parameters took the values given in Table 3. The results are shown in Fig. 19, from which it can be observed that there is a substantial influence of the rust expansion ratio (r_V). On the other hand, rust's molecular weight ratio (r_m) shows only a moderate effect, while the bulk modulus K_r, only causes a limited variation when it takes very low values (~0.2 kN.mm^2).

10. Conclusions

The model presented in this work only determines the time it takes for the concrete to crack *after* corrosion has initiated.

The presented model assumes volume compatibility to determine the pressure caused from rust products to cover. Volume equilibration allowed for the compaction of all materials affected by the pressure on cover, including rust.

A fracture mechanics concept, based on cover's strain energy has been introduced to identify cover failure. The rust properties assumed were based on experimental data on rust composition. A new rust

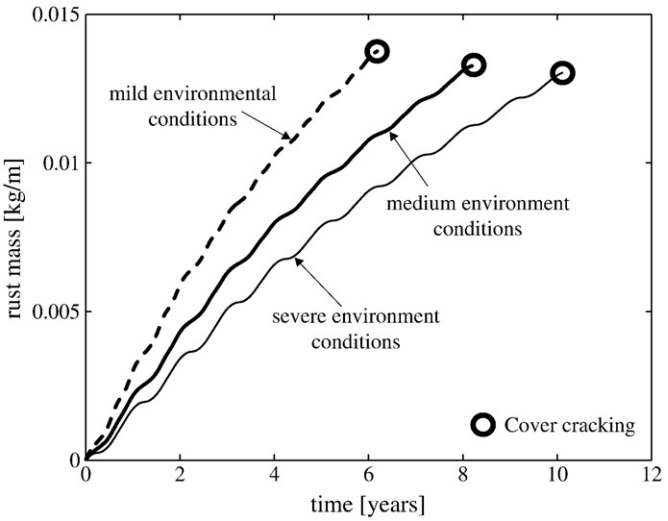

Fig. 17. Rust mass build-up under various environmental conditions, versus time.

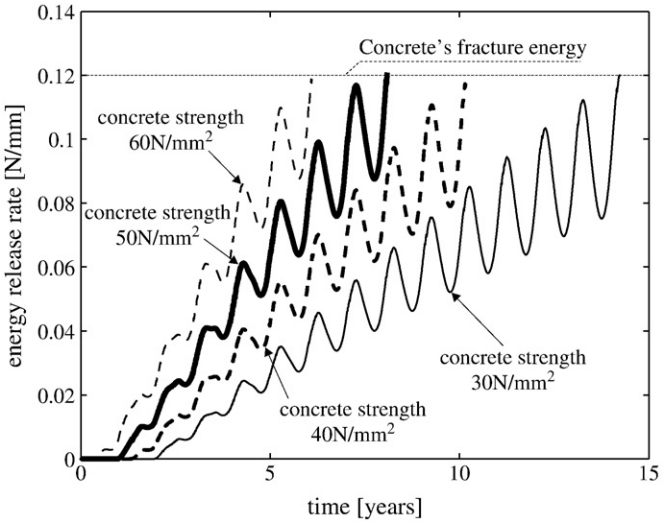

Fig. 18. Concrete strength and energy release rate build-up versus time.

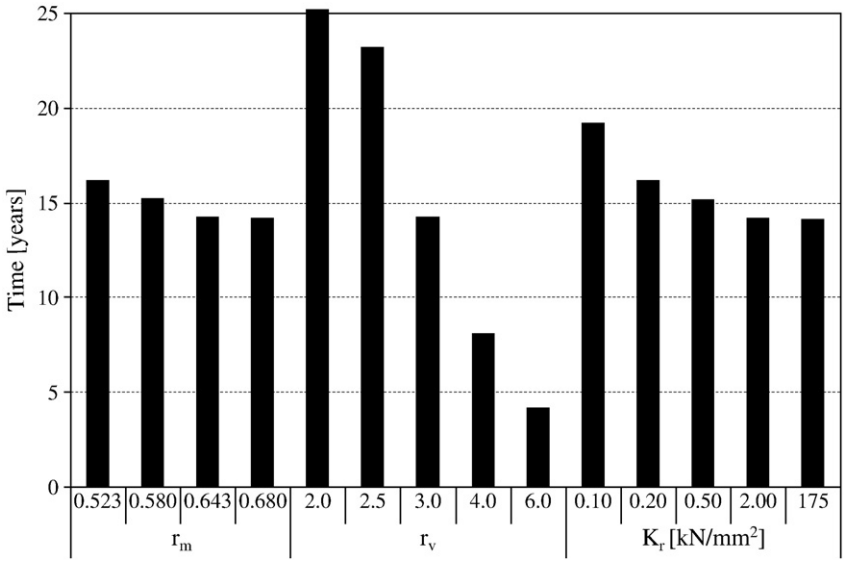

Fig. 19. Effect of rust properties on time to cover cracking.

production formula based on existing experimental evidence has also been introduced. The formula is a mixture of Faraday's Law and a formula proposed by Liu and Weyers. The latter was modified to account for change of rust layer diffusivity with thickening. Detailed concrete behavior has been introduced including tension softening and the effect of creep, which is important since the pressure exerted by rust is a long term loading.

As the main object of this work was to identify the environments under which structural lifetime is limited, the environmental conditions were carefully introduced and a parametric study was performed. The model reveals that time-to-cover-cracking is a function of rust production and resistance of the system to that production. The highest corrosion rates are towards the end of autumn and also towards the beginning of spring. On the other hand the highest resistance of the system to corrosion production is during summer, since the humidity levels reach low values. Therefore, structures with humidity levels close to 90% and high temperatures gave the shortest times to cover failure. In addition, structures exposed to humid summers would suffer from high rust production and rapid cover spalling.

The model also exposed behaviors that still have to be confirmed by experiments. It showed that rust pressure drops during summer due to creep. Water moves out of concrete and concrete deforms giving more space into which rust can expand. Stronger concrete cracks its cover sooner due to higher stiffness; the same rust volume translates to more pressure in stronger concrete. Further, the lower porosity means that a high proportion of the rust causes pressure on the cover, as less rust is needed to fill the pores. It was also found that tension softening has a marginal effect on cover cracking.

Rust volumetric ratio r_V gave an extensive influence on the output, while the molecular weight r_m gave an effect for values <0.6. Finally rust bulk modulus K_r affected time to cover failure only for low values (<0.3 kN/mm^2). Although research of rust composition is extensive, only one paper ([22]) gives the mass and volume properties. Because rust composition is a function of the environment, more research is needed in this field. The model presented here could then be updated with a formula that would give rust mass and volume properties as a function of h and T.

The model presented in this paper is deterministic; a more complete model would allow for the variation in the input parameters. However, there is still uncertainty even about the mean values of many of the parameters, to say nothing of their variability. If such knowledge could be obtained, it would be possible to apply Monte Carlo simulation to this analysis to determine probabilities of failure after various times.

References

[1] W. Wegner, M. Yaggi, Environmental impacts of road salt and alternatives in the New York City watershed, Stormwater 2 (5) (2001).
[2] I. Balafas, 2003. Fibre-reinforced-polymers vs steel in concrete bridges: structural design and economic viability. PhD thesis.
[3] C.J. Burgoyne, Rational use of advanced composites in concrete, Proceeding of the Institution of Civil Engineers: Structures and Buildings 146 (3) (2001) 253–262.
[4] I. Balafas and C. J. Burgoyne. Modelling the structural effects of rust on concrete cover. Submitted to ASCE Engineering Mechanics.
[5] Z. Bažant, Physical model for steel corrosion in concrete sea structures — theory, ASCE: Structural Journal 105 (ST6) (1979) 1137–1153.
[6] Y. Liu. Modelling the time-to-corrosion-cracking of the cover concrete in chloride contaminated reinforced concrete structures. PhD thesis, Virginia Polytechnic Institute and State University, 1996.
[7] S.J. Pantazopoulou, Modelling cover-cracking due to reinforcement corrosion in RC strustures, ASCE: Journal of Engineering Mechanics 127 (4) (2001) 342–351.
[8] K. Bhargava, A.K. Ghosh, Y. Mori, S. Ramanujam, Analytical model for time to cover cracking in rc structures due to rebar corrosion, Nuclear Engineering and Design 236 (2006) 1123–1139.
[9] T. Liu, R.W. Weyers, Modeling the dynamic corrosion process in chloride contaminated concrete structures, Cement and Concrete Research 28 (3) (1998) 365–379.
[10] Z. Bažant, Physical model for steel corrosion in concrete sea structures — application, ASCE: Structural Journal 105 (ST6) (1979) 1155–1166.
[11] F.J. Molina, C. Alonso, C. Andrade, Cover cracking as a function of bar corrosion: part II—numerical model, Materials and Structures 26 (1993) 532–548.
[12] R.E. Melchers, Modeling of marine immersion corrosion for mild and low-alloy steels — part 1: phenomenological model, Corrosion 59 (4) (2003) 319–334.
[13] R.E. Melchers, R. Jeffrey, Early corrosion of mild steel in seawater, Corrosion Science 47 (2005).
[14] B. Martin-Perez, 1999. Service life modelling of R.C. highway structures exposed to chlorides. PhD thesis, University of Toronto.
[15] T. El Maaddaay, K. Soudki, A model for prediction of time from corrosion initiation to corrosion cracking, Cement & Concrete Composites 29 (2007) 168–175.
[16] Y.X. Zhao, W.L. Lin, Modelling the amound of steel corrosion at the cracking of concrete cover, Advances in Structural Engineering 9 (5) (2006) 687–696.
[17] K. Bhargava, A.K. Ghosh, Y. Mori, S. Ramanujam, Modelling of time to corrosion-induced cover cracking in reinforced concrete structures, Cement and Concrete Research 35 (2005) 2203–2218.
[18] M. Ohtsu, S. Yosimura, Analysis of crack propagation and crack initiation due to corrosion of reinforcement, Construction and Building Materials 11 (7–8) (1997) 437–442.
[19] S.J. Williamson, L.A. Clark, Pressure required to cause cover cracking of concrete due to reinforcement corrosion, Magazine of Concrete Research 52 (6) (2000) 455–467.
[20] R.E. Melchers, Mathematical modelling of the diffusion controlled phase in marine immersion corrosion of mild steel, Corrosion Science 45 (2003).
[21] P. Konopka, Structural properties of rust, Fourth-year Undergraduate Project, University of Cambridge, 2005.
[22] K. Suda, S. Misra, K. Motohashi, Corrosion products of reinforcing bars embedded in concrete, Corrosion Science 35 (5–8) (1993) 1543–1549.

[23] T. Liu, R.W. Weyers, Modeling the time-to-corrosion cracking in chloride contaminated concrete structures, ACI: Materials Journal 95 (6) (1998) 675–681.
[24] W. López, J.A. González, Influence of the degree of pore saturation on the resistivity of concrete and the corrosion rate of steel reinforcement, Cement and Concrete Research 23 (2) (1993) 368–376.
[25] R. Tepfers, Cracking of concrete cover along anchored deformed reinforcing bars, Magazine of Concrete Research 31 (106) (1979) 3–12.
[26] B. Martin-Perez, H. Zibara, R.D. Hooton, M.D.A. Thomas, A study of the effect of chloride binding on service life predictions, Cement and Concrete Research 30 (2000) 1215–1223.
[27] M. Raupach, Chloride induced microcell corrosion of steel in concrete — theoritical background and practical consequences, Construction and Building Materials 10 (5) (1996) 329–338.
[28] Y. Liu, R. Weyers, Time to cracking for chloride-induced corrosion in reinforced concrete, in: C. Page, P. Bamforth, J. Figg (Eds.), Corrosion of Reinforcement in Concrete Construction, The Royal Society of Chemistry, 1996, pp. 88–104.
[29] C. Alonso, C. Andrade, J.A. González, Relation between resistivity and corrosion rate of reinforcements in carbonated mortar made with several cement types, Cement and Concrete Research 18 (5) (1988) 687–698.
[30] W.J. McCarter, H. Ezirim, M. Emerson, Properties of concrete in the cover zone: penetration, sorptivity and ionic ingress, Magazine of Concrete Research 48 (176) (1996) 149–156.
[31] N.R. Buenfeld, J.B. Newman, The permeability of concrete in a marine environment, Magazine of Concrete Research 36 (127) (1984) 67–80.
[32] K. Tuutti. Service life of structures with regard to corrosion of embedded steel. In ACI, editor, Performance of Concrete in Marine Environment, International Conference Proceedings (SP-65), pages 223–236, 1980.
[33] K. Okada and T. Miyagawa. Chloride corrosion of reinforcing steel in cracked concrete. In ACI, editor, Performance of Concrete in Marine Environment, International Conference Proceedings (SP-65), pages 237–254, 1980.
[34] J.P. Broomfield, Corrosion of Steel in Concrete, 1 editionE & FN Spon, 1997.
[35] C. Andrade, C. Alonso, Corrosion rate monitoring in the laboratory and on-site, Construction and Building Materials 10 (5) (1996) 315–328.
[36] T.D. Maarcotte, C.M. Hansson, The influence of silica fume on the corrosion resistance of steel in high performance concrete exposed to simulated sea water, Journal of Materials Science 38 (2003) 4765–4776.
[37] G.S. Duffo, W. Morris, I. Raspini, C. Saragoni, A study of steel rebars embedded in concrete during 65 years, Corrosion Science 46 (2004).
[38] O. Poupard, V.L. Hostis, S. Catinaud, I. Petre-Lazar, Corrosion damage diagnosis of a reinforced concrete beam after 40 years natural exposure in marine environment, Cement and Concrete Research 36 (2006).
[39] S. Care, A. Raharinaivo, Influence of impressed current on the initiation of damage in reinforced mortar due to corrosion of embedded steel, Cement and Concrete Research 37 (2007) 1598–1612.
[40] S. Care, Q.T. Nguyen, V.L. Hostis, Y. Berthaud, Mechanical properties of therust layer induced by impressed current method in reinforced mortar, Cement and Concrete Research 38 (2008) 1079–1091.
[41] T.D. Maarcotte, C.M. Hansson, Corrosion products that form on steel within cement paste, Materials and Structures 40 (2007) 325–340.
[42] C. Andrade, C. Alonso, F.J. Molina, Cover cracking as a function of rebar corrosion: part I — experimental test, Materials and Structures 26 (1993) 543-464.
[43] C.Q. Li, R.E. Melchers, J.J. Zheng, Analytical model for corrosion-induced crack width in reinforced concrete structures, ACI: Structural Journal 103 (4) (2006) 479–487.
[44] Y.Y. Chen, H.J. Tzeng, L.I. Wei, L.H. Wang, J.C. Oung, H.C. Shih, Corrosion resistance and mechanical properties of low-alloy steels under atmospheric conditions, Corrosion Science 47 (2005).
[45] J.F. Marco, M. Garcia, J.R. Gancedo, M.A. Martin-Luengo, G. Joseph, Characterization of the corrosion products formed on carbon steel after exposure to the open atmosphere in the antartic and easter island, Corrosion Science 42 (2000) 753–771.
[46] M. Benarie, F.L. Lipfert, A general corrosion function in terms of atmospheric pollutant concentrations and rain ph, Atmospheric Environment 20 (10) (1986) 1947–1958.
[47] A.A. Torres-Acosta, 1999. Cracking induced by localized corrosion of reinforcement in chloride contaminated concrete. PhD thesis, University of South Florida, College of Engineering, Department of Civil and Environmental Engineering.
[48] A.A. Torre-Acosta, A.A. Sagues, Concrete cracking by localised steel corrosion — geometric effects, ACI, Materials Journal 101 (6) (2004) 501–507.
[49] Q.T. Nguyen, A. Millard, S. Care, V. L'Hostis, Y. Berthaud, Fracture of concrete caused by the reinforcement corrosion products, Journal of Physics IV France 136 (2006) 109–120.
[50] J.W. Hutchinson, Z. Suo, Mixed mode cracking in layered materials, in: J.W. Hutchinson, T.Y. Wu (Eds.), Advances in Applied Mechanics, 1992, pp. 63–91.
[51] P.M.M. Achinta, C.J. Burgoyne, Fracture mechanics of plate debonding, ASCE: Journal of Composites for Construction 12 (4) (2008) 396–404.